Reactivity of Atomic Cobalt with Molecular Oxygen: A Combined IR Matrix Isolation and Theoretical Study of the Formation and Structure of CoO_2

Delphine Danset, Mohammad E. Alikhani, and Laurent Manceron*

LADIR/Spectrochimie Moléculaire CNRS UMR 7075, Université Pierre et Marie Curie, case 49, 4 place Jussieu 75252 Paris, France

Received: June 19, 2004; In Final Form: August 26, 2004

The reactivity of atomic cobalt toward molecular oxygen in rare gas matrices has been reinvestigated. Experiments confirm that Co atoms in their a^4F ground state are inert toward O_2 in solid argon and neon but reactive in the b^4F first excited state, in agreement with the previous gas-phase study of Honma and co-workers. The formation of CoO_2 starting from effusive beams of Co and O_2 has been followed by IR absorption spectroscopy, both in neon and argon matrices. Our observations show that only the dioxo form, OCoO, is stabilized in the matrix and that IR absorptions previously assigned to the peroxo and superoxo forms are due to other, larger species. The present data strongly support the linear geometry in rare gas matrices proposed by Weltner and co-workers. We report on measurements on all IR-active fundamental modes for $^{16}OCo^{16}O$, $^{18}OCo^{18}O$, and $^{16}OCo^{18}O$ with additional combination transitions supplying anharmonicity correction. This allows for a 5.93 ± 0.02 mdyne/Å CoO harmonic bond force constant in solid neon. Using the empirical relationship previously optimized for the CoO diatomics, an approximate value for the CoO internuclear bond distance is proposed (1.615 ± 0.01Å). In light of recent theoretical studies predicting $^2A_1$ or $^6A_1$ electronic ground states, the geometry and electronic structure of the OCoO molecule has also been reconsidered. Calculations carried out at the CCSD(T)/6-311G(3df) level indicate a linear structure with an $r_e = 1.62$ Å bond distance, consistent with the experimental estimate. For later studies of larger systems, where CCSD(T) calculations become too time-consuming, an effective DFT-based method is proposed which reproduces the basic electronic and geometrical properties of cobalt dioxide. Quantitative results are compared to the experimental data and high-level results regarding bond length and frequencies. This DFT method is used to propose a reaction pathway.

Introduction

Bulk cobalt surfaces are known to be very reactive to molecular oxygen exposure,[1] yet large differences are observed between what happens on metal surfaces and at the atomic scale. The specific reaction of an isolated cobalt atom toward an oxygen molecule has been quite controversial and given rise to conflicting experimental and theoretical works in the past years.

Van Zee et al.[2] first studied the Co + O_2 reaction in argon matrices and established by electron spin resonance (ESR) spectroscopy that the dioxo form of CoO_2 is linear with a $^2\Sigma^+$ ground state. Their attempts to observe any M−O_2 precursor of peroxo or superoxo form were not successful, leading them to conclude that no other chemically bound form of CoO_2 than the linear molecule (dioxo form) was stabilized in an argon matrix. Additionally, it appeared that the unpaired electron of the Co atom remained in the vicinity of the cobalt nucleus in a molecular orbital of strong 4s character and did not significantly participate in the molecular bond.

Matsui et al.[3] followed the kinetics of depletion by O_2 of ground, first, and second excited states of Co (a^4F, b^4F, and ^2F, respectively) in the gas phase in a flow reactor and proved that, if Co atoms in their first or second excited states could react with O_2 on the scale of a few tens of collisions, the ground state was not reactive toward molecular oxygen. Their technique did not access the nature of the reaction products; therefore, only the atomic reactivity was discussed.

Chertihin et al.[4] studied the reaction products of laser-ablated cobalt atoms and molecular oxygen isolated in solid argon. They reported the observation of three states or forms corresponding to isomeric structures of CoO_2, linear, cyclic, or end-on, and used density functional theory (DFT) calculations to support their assignments. They note that all of the complexes are formed during deposition, but that the very high energy brought by the laser ablation could be an important factor. The dioxo form was characterized by the observation of the asymmetric stretching mode (ν_3) and one combination ($\nu_1 + \nu_3$). The other structures were characterized by O═O stretching modes at 984 cm^{-1} for the cyclic form and at 1286 cm^{-1} for the end-on form.

DFT studies have been carried out by several groups: Gutsev et al.[5] performed a systematic study of the dioxo, peroxo, and superoxo isomers of 3d transition metal atoms and their anions at the BPW91 level. According to their results for cobalt oxides, the peroxo and superoxo forms correspond to metastable states, respectively, 1.86 and 1.88 eV above the most stable dioxo form. For the dioxo form, the optimized ground-state electronic and geometric structure is a $^2A_1$ state with an OMO angle of 154°, in contradiction with the conclusions of refs 2 and 4. In general, calculations on cobalt dioxide seem to have met an array of difficulties arising from all the low-lying electronic states and near-degeneracy effects. Uzunova et al.[6,7] studied CoO_n (n = 1−4) cobalt clusters and their excited states with the B1LYP exchange correlation functional. In their calculations, the $^2\Sigma_g^+$ state of OCoO is a transition state, 150 cm^{-1} higher in energy than the two symmetrically located bent $^2A_1$ configurations.

* To whom correspondence should be addressed. E-mail: lm@ccr.jussieu.fr.

10.1021/jp047327x CCC: $30.25
Published on Web 12/15/2004

Moreover, the true ground state (about 0.6 eV below the doublet) would belong to the sextet manifold, $^6A_1$, with an almost linear geometry (179.9°). Fairly long Co−O bonds (1.745 Å) are predicted, and frequencies at 184 (a_1), 528 (b_2), and 635 (a_1) cm^{-1} (with respective IR intensities of 41, 18, and 0 km/mol) are calculated for the ground state, in complete disagreement with experimental observations.

In this paper, several important points will be addressed. First, is the reactivity of ground- and excited-state cobalt atoms toward molecular oxygen fundamentally different in rare gas matrices and in the gas phase? If so, are peroxide structures intermediates in the reaction as seen for other systems[8] such as Ni + O_2 or Pt + O_2?

Second, can we add to our knowledge of the OCoO molecule structure by obtaining new spectroscopic data, and what level of quantum chemical calculation is necessary to reproduce basic electronic and geometrical properties? Comparisons with other dioxide molecules such as ONiO will also be presented.

Experimental and Computational Methods

The samples were formed by co-condensing Co vapor and dilute O_2−Ar or Ne mixtures (0.5−16% O_2/Ar or 200−2000 ppm O_2/Ne) onto one of six flat, highly polished, Rh-plated copper mirrors maintained between 3 and 15 K using a pulse-tube, closed-cycle cryogenerator (Cryomech PT405, U.S.A.).[9] The system was evacuated at a base pressure of about 7×10^{-8} mbar before refrigeration of the sample holder. The metal-atom source was a tungsten filament wetted with Co and heated to 1400−1600 °C, generating the metal vapor. The metal deposition rate was carefully monitored with the aid of a quartz microbalance and varied from 9 to 20 nmol/min.

High-purity argon (Air Liquide, France; 99.995%)/neon (Air Liquide, France; 99.9995%), $^{16}O_2$ (Air Liquide, France; 99.998%), and $^{18}O_2$ (Isotec, U.S.A.; 99.0% ^{18}O) were used to prepare the O_2−Ar/Ne mixtures. To prepare scrambled oxygen ($^{16}O^{18}O$), equal quantities of $^{16}O_2$ and $^{18}O_2$ were scrambled in a Tesla discharge for approximately 10 min, the mixture then containing 25% $^{16}O_2$, 50% $^{16}O^{18}O$, and 25% $^{18}O_2$. The gas inlet line was driven through a liquid nitrogen trap within the vacuum system, thereby condensing impurities in the mixture and precooling it to about 77 K before reaching the mirror.

In general, after 90−120 min of deposition, IR spectra of the resulting samples were recorded in the transmission−reflection mode between 5000 and 15 cm^{-1} using a Bruker 120 FTIR spectrometer. In the far-IR region (80−600 cm^{-1}), a globar source, an Si/Mylar composite beam splitter, and an He-cooled Si−B bolometer with a 4 K-cooled 660 cm^{-1} low-pass filter were used. For the very far-IR region (15−100 cm^{-1}), the source was a mercury medium-pressure arc lamp, and the bolometer was used with a 4 K-cooled 110 cm^{-1} low-pass filter. In the mid-IR region (500−5000 cm^{-1}), a Ge/KBr beam splitter was used along with an N_2-cooled narrow-band HgCdTe photoconductor. Mid-, far-, and very far-IR spectra were collected on the same samples. Wedged CsI and polyethylene windows were mounted on a rotatable flange separating the interferometer vacuum (5×10^{-4} mbar) from that of the cryostatic cell (10^{-8} mbar). The resolution was varied from 0.05 to 0.5 cm^{-1}. Bare mirror backgrounds, recorded prior to sample deposition, were used as references in processing the sample spectra. The spectra were subsequently subjected to baseline correction to compensate for IR light scattering and interference patterns.

Photoexcitations were performed through a CaF_2 window mounted on the assembly. In the IR region, a 150 W globar lamp was used with a large parabolic collection mirror, and the unfiltered irradiation power was measured around 950 mW/cm^2, which is estimated to be about 60 times that of the spectrometer source. High/low- and band-pass filters were used to narrow down the photoexcitation ranges and obtain the specific energy responsible for photoactive reactions among the species. By using a 4500−3900 cm^{-1} band-pass filter, photoexcitation with 40 mW/cm^2 was routinely achieved, and irradiations were performed for 30−60 min. For UV−vis irradiations, an HgXe high-pressure arc lamp was used with a converging lens focusing the light on the sample, and the duration of the irradiation varied from 15 to 30 min. Total UV power was measured in the order of magnitude of 200 mW/cm^2 in the 220−420 nm range. Broadband photoexcitation was performed, because active photons were outside the intervals isolated by narrow Hg line filters.

Alternatively, for some experiments, narrow band (5−6 cm^{-1} line width) photoexcitations were performed using the idler beam of an optical parametric oscillator (OPO) source operating with a β-barium borate (BBO) crystal, pumped by the third harmonic of an Nd:YAG laser (OPOTEK, QUANTEL), delivering 0.5 mJ light pulses at 20 Hz, continuously tunable in the 12 500−4300 cm^{-1} range.

Theoretical calculations have been performed with the *Gaussian 03* quantum chemical package[10] using a DFT approach and the coupled cluster method including single and double substitutions and triple excitations noniteratively (CCSD(T)), within the frozen core approximation and using unrestricted wavefunction. The DFT calculations have been carried out by combining Becke's exchange[11] and Perdew−Wang's correlation functionals[12] (denoted BPW91). The standard 6-311G basis set[13−15] augmented by 2d and 3df polarization functions was used for all atoms. The scalar relativistic effect has been calculated at the BPW91/6-311G(3df) level using the Douglas−Kroll−Hess second-order method as implemented in the *Gaussian 03* package.

Experimental Results

Samples were made by cocondensation of thermally evaporated cobalt atoms and an O_2−rare gas mixture onto a highly polished mirror maintained at cryogenic temperatures. Co/Ar and O_2/Ar molar ratios were varied 0.2−1‰ and 0.5−8%, respectively. In neon, concentrations were decreased to compensate for easier atomic and molecular diffusion. The O_2/Ne and Co/Ne molar ratios were varied 200−2000 ppm and 50−500 ppm, respectively. The deposition temperature was varied 9−12 K in argon and 3−6 K in neon in order to favor CoO_2 formation and improve matrix transparency. Neon samples showed a lower product yield in monocobalt species compared to argon, but no qualitative change in the chemistry of the system was observed. Table 1 presents data obtained in both type of matrices.

Spectra taken directly after deposition show main absorptions due to small quantities of the insertion product OCoO (945.4 cm^{-1}) and to Co_2O_2 [4] (685 cm^{-1}) (see Figure 1a). Although there are signs of other complexes formed during deposition, concentration effects show that these weaker bands in the mid-IR region belong to larger species. In more concentrated samples (4−8% O_2−Ar or 2000 ppm O_2−Ne), the 984.9 cm^{-1} band, assigned to a $Co(O_2)$ superoxide by Chertihin et al., was multiplied by 5 when O_2 concentration was doubled, clearly indicating that this molecule contains much more than just one oxygen molecule; it cannot therefore be a $Co(O_2)$ superoxide species. The absorption band at 1286.1 cm^{-1} (labeled X on

TABLE 1: Frequencies (cm^{-1}) for OCoO in Argon and Neon Matrix[a]

	$^{16}OCo^{16}O$		$^{18}OCo^{18}O$		$^{16}OCo^{18}O$	
	Ar	Ne	Ar	Ne	Ar	Ne
ν_1	783.7[b] (0)	796.2[b]	740.9[b]	751.5[b]	760.6 (0.012)	771.1[b]
ν_2	82.8 (0.13)		78.5		81.4 (0.14)	
ν_3	945.4[c] (1)	954.7	911.0[c]	920.7	930.4[c] (1)	941.2
$\nu_1 + \nu_3$	1717.4[c] (0.04)	1739.2	1640.2[c]	1660.9	1679.3[c] (0.04)	1700.6

[a] Relative intensities are in parentheses. [b] Calculated by $(\nu_1 + \nu_3)_{exp} - \nu_{3\ exp}$ using the anharmonic term $X_{13} = -11.7\ cm^{-1}$ obtained from $^{16}OCo^{18}O$. [c] Observed previously in ref 4.

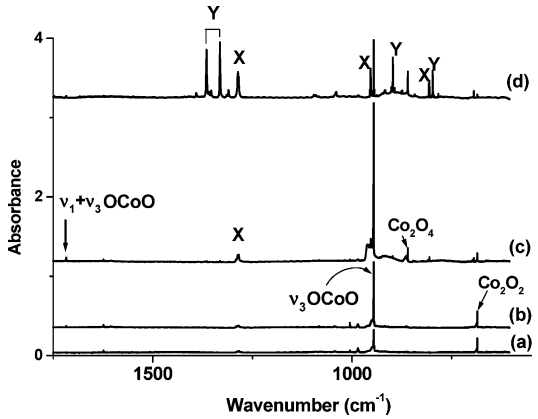

Figure 1. IR spectra in the 800−2000 cm^{-1} region for thermally evaporated Co atoms codeposited with 2% $^{16}O_2$ in argon at 9 K: (a) deposition, (b) broadband IR irradiation, (c) broadband UV photolysis, (d) annealing to 30 K.

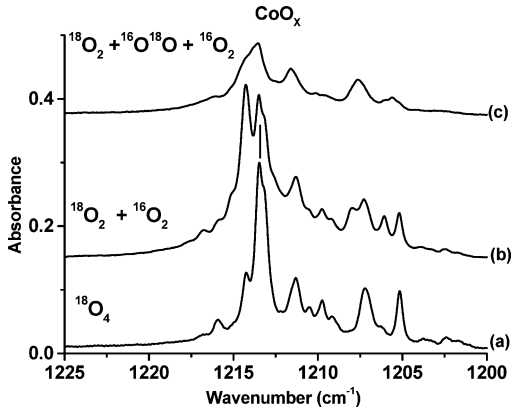

Figure 2. IR spectra in the 1200−1225 cm^{-1} region for thermally evaporated Co atoms codeposited with 1000 ppm O_2 in neon. CoO_4 fundamental absorption with different isotopic precursors: (a) Co + $^{18}O_2$, (b) Co + $^{16}O_2$ + $^{18}O_2$, (c) Co + $^{16}O_2$ + $^{16}O^{18}O$ + $^{18}O_2$.

Figure 1) was also assigned to a $Co(O_2)$ peroxide but with an asymmetric structure. It is present in our samples but showed, likewise, a quadratic dependence to O_2 concentration. It also grew considerably upon UV irradiation and, yet again, after annealing the sample to 25 K. In samples containing ($^{16}O_2$ + $^{18}O_2$) precursors, the observed isotopic pattern is a quartet, clearly resolved at 0.1 cm^{-1} resolution (Figure 2). In matrices containing a ($^{16}O_2$ + $^{16}O^{18}O$ + $^{18}O_2$) mixture, this band presents a more complex structure than expected for a molecule containing one O_2 molecule, confirming that species X is larger than a CoOO peroxide. The spectroscopic properties, as well as the photophysics of this molecule, will be developed in the following article. Nonetheless, it is important to emphasize that the conclusions mentioned in ref 4 must be revised.

In argon, the presence of OCoO can be traced in the mid-IR region by the ν_3 asymmetric stretching mode at 945.4 cm^{-1}, as well as the $\nu_1 + \nu_3$ combination at 1717.4 cm^{-1} already assigned

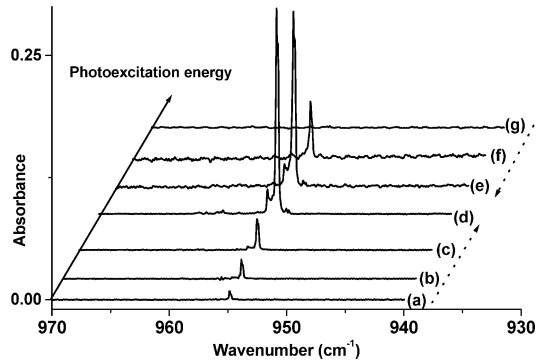

Figure 3. IR spectra in the ν_3 region of OCoO isolated in neon (Co/Ne = 200 ppm; O_2/Ne = 500 ppm). Effects of IR irradiation using combinations of high-pass and low-pass filters. Each spectrum is the difference between after and before irradiation in different energy ranges: (a) $\tilde{\nu} < 2050\ cm^{-1}$, (b) $\tilde{\nu} < 2740\ cm^{-1}$, (c) $\tilde{\nu} < 3400\ cm^{-1}$, (d) $\tilde{\nu} < 4500\ cm^{-1}$, (e) $\tilde{\nu} \in [2200-4500]\ cm^{-1}$, (f) $\tilde{\nu} \in [4000-5400]\ cm^{-1}$, (g) $\tilde{\nu} > 6000\ cm^{-1}$.

in ref 4. In neon matrices, these absorptions are blue-shifted to 954.7 and 1739.2 cm^{-1}, respectively. These bands grow considerably upon either IR or UV irradiation (Figure 1b,c). In neon, the responses to IR and UV irradiations are the same as in argon, but again, the product yield is lower than in argon.

Combinations of optical filters were used to isolate different IR energy ranges to perform more selective irradiations. Several separate samples of identical concentration, deposition time, and temperature were necessary for these experiments to avoid saturation effects, as the process is not reversible. IR photoexcitations were led until the maximum yield of CoO_2 was obtained. Therefore, as it can be seen in Figure 3, spectra a−d were obtained on a first sample irradiating with increasing energy, and then, spectra g−e were obtained on a second sample irradiating with decreasing energy. These effects show that OCoO formation is induced in great majority by photons of the 3800−4000 cm^{-1} energy range. Note that spectrum 3a was taken after IR irradiation but without filtering the light of the spectrometer above 1750 cm^{-1} as it was for the other spectra. The slight observable growth of OCoO is induced by the light of the spectrometer source and can be considered an artifact, but it is left here to show the maximum modification induced by probing the sample with an unfiltered IR spectrometer beam. The 4500−10 000 cm^{-1} range was also probed using the tunable light from an OPO, and a second energy range leading to OCoO formation could be located around 7450 ± 25 cm^{-1}. Although a precise comparison of the quantum yields between the two domains is difficult, the higher energy range seemed about a factor of five less efficient than the mid-IR excitation. No other species showed comparable variations following these irradiations, and careful examination over the entire spectral range failed to reveal any IR absorption potentially due to chemically bonded Co−O_2 precursor of OCoO.

UV-broadband photoexcitation was also performed and induced formation of OCoO in high yield, but also small

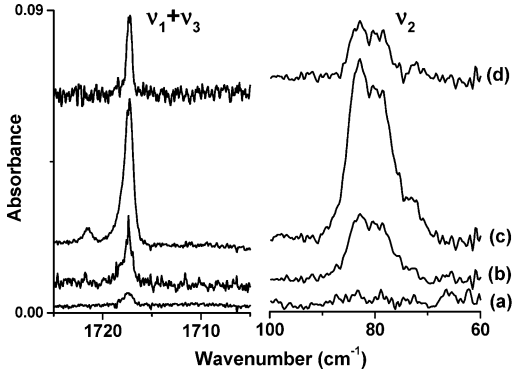

Figure 4. IR spectra in the ($\nu_1 + \nu_3$) and ν_2 regions of OCoO isolated in argon: (a) deposition, (b) IR irradiation, (c) broadband UV irradiation, (d) annealing to 30 K.

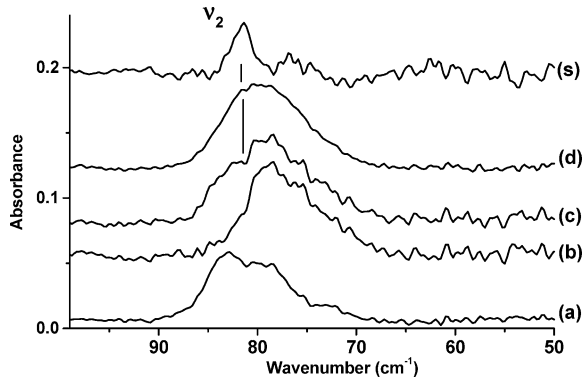

Figure 5. IR spectra in the ν_2 region of OCoO isolated in argon: (a) Co + $^{16}O_2$, (b) Co + $^{18}O_2$, (c) Co +$^{16}O_2$ + $^{18}O_2$, (d) Co + $^{16}O_2$ + $^{16}O^{18}O$ + $^{18}O_2$, (s) subtraction [d − (a + b)]/2.

quantities of other, larger species that will be discussed in the next and later articles (Figure 1c). Upon annealing the sample to 35 K, OCoO decreased by more than half (Figure 1d) giving way to larger species. When annealing the sample directly after deposition, without any photoexcitation, no formation of OCoO was observed.

In the very far-IR region, a broad and asymmetrical band at 82.8 ± 0.5 cm^{-1} (fwhm ≈ 10 cm^{-1}) was observed and showed an identical behavior to that of the OCoO ν_3 fundamental and $\nu_1 + \nu_3$ combination (Figure 4). It grew upon IR irradiation and UV broadband photolysis only to disappear after annealing, thus showing similar behavior to the other OCoO absorptions.

When $^{16}O_2$ was replaced by $^{18}O_2$ in argon, the 945.4 and 1717.4 cm^{-1} bands were respectively shifted to 911.0 and 1640.2 cm^{-1} as seen in ref 4, and the 82.8 ± 0.5 cm^{-1} absorption shifted to 78.5 ± 0.5 cm^{-1} (Figures 4 and 5). In neon matrices, the 954.7 and 1739.2 cm^{-1} bands were shifted to 920.7 and 1660.9 cm^{-1}. In samples containing an equal 50%−50% mixture of $^{16}O_2$ and $^{18}O_2$, a doublet structure was observed for all bands. Finally, in samples containing $^{16}O_2$, $^{16}O^{18}O$, and $^{18}O_2$ precursors, symmetric triplet structures were observed, with intermediate components at 930.4, 1679.3, and 81.4 ± 0.5 cm^{-1} in argon, thus confirming that the 82.8 cm^{-1} absorption belongs to a species containing only one oxygen molecule and that the oxygen atoms are equivalent. Additionally, a weak band at 760.4 cm^{-1} is present (Figure 6), which only appears in samples containing $^{16}O^{18}O$ molecules. This weak band grows upon IR and UV irradiation identically to the absorption bands of OCoO but is overlapped by absorptions of larger species when the sample is annealed. Concentration effects for this band show a linear dependence to Co and O_2 concentrations, and in samples

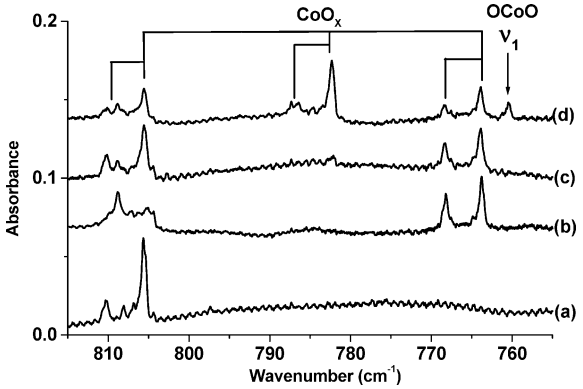

Figure 6. IR spectra in the 755−815 cm^{-1} region for thermally evaporated Co atoms codeposited with 2% O_2 in argon at 9 K: (a) Co + $^{16}O_2$, (b) Co + $^{18}O_2$, (c) Co + $^{16}O_2$ + $^{18}O_2$, (d) Co + $^{16}O_2$ + $^{16}O^{18}O$ + $^{18}O_2$.

in which the quantity of OCoO is weak, this band is not observable.

Formation Pathway and Vibrational Spectrum of Cobalt Dioxide

Both the formation pathway and the structure of the dioxo−CoO_2 molecule have been quite controversial. Concerning the first point, the two main questions are as follows: Do ground-state cobalt atoms react with molecular oxygen in rare gas matrices? Is the Co + O_2 reaction a direct insertion?

In the gas-phase, Matsui et al.[3] established that Co atoms do not react in their ground state but in their first or second excited states, b^{4}F and a^{2}F, some 3500 and 7500 cm^{-1}, respectively, above the ground state, with some differences between spin−orbit sublevels.

In their matrix ESR study, Van Zee et al. only observed the insertion product and concluded the absence of formation of an $M^+O_2^-$ complex. They were careful to use both thermal evaporation and laser ablation as means of producing CoO_2 molecules, knowing that the latter technique was very highly energetic and could have destroyed possible metastable forms of CoO_2 before they could be stabilized in the argon matrix. Nonetheless, only OCoO was stabilized, and the ESR spectra evidenced a $^2\Sigma$ ground state. As stated already, absorptions assigned in ref 4 to other possible superoxide and asymmetric peroxide structures isolated in solid argon, in fact, belong to larger species than CoO_2. In our experiments, we did not detect any IR absorption assignable to an intermediate Co + O_2 precursor. A possible reason would be that the vibration of a hypothetical Co(O_2) complex would be too weak to be detected here, but given the conclusion of ref 2 and the fact that the energy range necessary to induce formation of the product corresponds to energies close to electronic excitations of Co atoms, it seems much more likely that the precursor is a Co − O_2 unbound pair or, at most, very weakly bonded by van der Waals interactions.

Although the cobalt atoms were thermally evaporated in order to avoid high electronic excitation, we nonetheless observe formation of a small amount of OCoO directly after deposition (Figure 1b, 15% of the total quantity). Using Boltzmann's distribution law and the source temperature around 1770 K, we can estimate that 6% of the cobalt atoms are emitted in the b^{4}F excited state and 0.3% in the ^{2}F state but, given the transit time of several milliseconds necessary to reach the sample, it seems unlikely that the reaction with metastable Co atoms is responsible for the observed OCoO. Rather, a more probable explana-

TABLE 2: Comparison of Experimental and Reported Calculated Frequencies (cm^{-1}) for CoO_2 Isomers (IR Intensities in Parentheses, km/mol)

	OCoO		CoO_2		CoOO	
exptl[a]	$^2\Sigma$	Π 82.8				
		Σ_u 945.4				
		Σ_g 783.7				
BPW91[5]	$^2A_1$	a_1 116	$^2A_2$	a_1 610	$^4A'$	a′ 189
		b_2 1042		b_2 1023		a′ 509
		a_1 895		a_1 1007		a′ 858
B1LYP[6]	$^6A_1$	a_1 184 (41)	$^4A_1$	a_1 898 (184)	$^2A'$	a′ 201 (8)
		b_2 528 (18)		b_2 323 (7)		a′ 476 (5)
		a_1 635 (0)		a_1 311 (70)		a′ 1126 (582)
B3LYP[4]	$^2A'$	a_1 160 (31)	$^4A_1$	a_1 903 (127)	$^2A'$	a′ 182 (7)
		b_2 994 (99)		b_2 320 (0.6)		a′ 466 (4)
		a_1 793 (12)		a_1 441 (7)		a′ 1136 (599)
BP[4]	$^2A_1$	a_1 132 (20)	$^4A'$	a′ 226 (45)	$^2A'$	a′ 196 (5)
		b_2 1075 (174)		a′ 546 (14)		a′ 489 (5)
		a_1 992 (11)		a′ 885 (210)		a′ 1140 (340)
CASSCF[4]	$^2\Delta_g$	Π 138 (66)	$^4B_2$	a_1 1063 (2)	$^2A'$	a′ 101 (6)
		Σ_u 896 (121)		b_2 327 (3)		a′ 552 (89)
		Σ_g 611 (0)		a_1 468 (96)		a′ 1029 (47)

[a] In solid argon, this work and ref 4.

tion is sample exposure to the IR light emitted by the hot metal source during deposition. Annealing the sample to 20 K in the dark directly after deposition allows the cobalt atoms and O_2 molecules to diffuse in the crystal. If Co reacted in the ground state, this procedure should lead to the formation of OCoO by diffusion only, as observed with other metal atoms.[8] Spectra taken after annealing and filtering light above 1750 cm^{-1} showed that the initial quantity of OCoO remained unchanged. No other isomer of CoO_2 was observed at any stage of the experiments (after irradiation or annealing). Again, the precursors appear to be cobalt atoms and oxygen molecules that had not reacted during deposition, and remained isolated in the matrix in proximity to each other, as the energies efficient at promoting the reaction (3800−4000 cm^{-1} and near 7450 cm^{-1}) match relatively well the $a^4F \rightarrow b^4F$ and $a^4F \rightarrow {}^2F$ gas-phase transition energies of atomic Co.

Matsui et al. were able to prove that Co atoms prepared in the b^4F or ^2F states are about equally reactive toward molecular oxygen, but excitation in the energy range corresponding to the upper state was not as efficient in our experiments. This is possibly because the $a^4F \rightarrow {}^2F$ optical transition is both electric dipole- and spin-forbidden, making the ^2F level more difficult to populate by direct optical excitation. We searched but did not observe these forbidden atomic IR transitions. Both are too weak to be observed here or perhaps broadened by the influence of the matrix. Note that probing the existence of very weak electronic transitions by following the formation of photoproducts following selective electronic excitation has been evidenced before, for instance, in the study of Frei and Pimentel[13] of low-energy reaction pathways in the reaction of O_2 in its $^1\Delta_g$ state with substituted furans or molecular fluorine.

UV broadband photoexcitation proved to be very effective in forming more OCoO molecules. The Co atoms are highly excited and, given the many closely spaced excited states in the UV−vis region,[16] isolating the reactive state is not possible here. Indeed, the atom can reach many highly excited states by the nonselective broadband irradiation and relax into a variety of lower states before reaction with O_2 is induced.[3] Furthermore, broadband photoexcitation could induce diffusion in rare gas matrices due to temperature elevation caused by the strong UV−vis absorptions of the precursors. Thereby, no conclusive result can be extracted from this irradiation, except maybe that the IR irradiation is useful on precursors that are adjacent in the matrix, and the broadband photolysis allows more distant precursors to diffuse and react, leading to further OCoO formation.

TABLE 3: Comparison of Empirical Harmonic Force Constants (mdyn/Å) Calculated for Co and Ni Mono- and Dioxides with Measured and Estimated Bond Lengths (Å)

	OCoO[a]	ONiO	NiO	CoO
MO bond constant	5.93	5.280[b]	5.034	5.305
interaction constant	0.23	−0.270		
r_e	1.615 ± 0.010[a]		1.627[b]	1.631[e]

[a] This work. [b] From ref 8. [c] From force constant vs distance correlation, ref 9. [d] From ref 20. [e] From ref 19.

The structure of this molecule has also been controversial. The ESR study by Van Zee et al. deduced a linear geometry with a $^2\Sigma_g^+$ ground state,[2] but this conclusion has been contradicted in recent theoretical studies.[5−7]

We report here observations of the bending mode (ν_2) of OCoO near 80 cm^{-1} for all isotopomers in argon. The bending mode has a very low energy, in poor agreement with the predictions of refs 5−7 made for bent structures (Table 2). Moreover, the observed isotopic effects are consistent with a linear geometry. The 760.4 cm^{-1} absorption band in solid argon is assigned to the ν_1 fundamental of $^{16}OCo^{18}O$, IR-activated because of the symmetry lowering. Along with the observation of the $\nu_1 + \nu_3$ combination, we are able to obtain the crossed anharmonic term, $X_{13} = -11.7$ cm^{-1}, and thereby predict the frequency of the ν_1 fundamental for the $^{16}OCo^{16}O$ molecule at 783.7 cm^{-1} in argon and 796.2 cm^{-1} in neon. These values are in excellent agreement with unpublished reports by Wang et al.,[17] who placed the ν_1 (symmetric stretch) of $^{16}OCo^{16}O$ at 790 ± 60 cm^{-1} from a progression observed in photodetachment spectroscopy experiments. Careful examination of the spectra taken on samples containing only one isotopic precursor ($^{16}O_2$ or $^{18}O_2$) shows no absorption band at the predicted frequencies. Experimental data show that ν_1 in $^{16}OCo^{18}O$ is very weak, about one-third of the integrated intensity of the $\nu_1 + \nu_3$ combination. Nevertheless, the observation is made in samples containing the three isotopic precursors and, thus, ν_1 should easily be observed in samples containing only $^{16}OCo^{16}O$ or $^{18}OCo^{18}O$, if ν_1 were IR active. We also note that the first overtone of the very strong ν_3 mode is not observable. Therefore, we consider all this definitive evidence of the linearity of OCoO in rare gas matrices.

A simple harmonic force-field calculation with a fixed linear geometry, $F_{CoO} = 5.93$ and $F_{CoO,CoO} = 0.23$ mdyn/Å force constants, reproduces the isotopic shifts on the two stretching modes within 0.3 cm^{-1} of the experimental data. On the basis of the supplementary assumption of CoO bond dipole moment additivity, the eigenvectors would predict the IR intensity ratio between ν_1 and ν_3 of 0.9% in $^{16}OCo^{18}O$, when experimental measurements give 1.2 ± 0.3%, in acceptable agreement. The CoO bond force constant for OCoO can be compared to the CoO diatomics value ($F_{CoO} = 5.305$ mdyne/Å), indicating that the bond is stronger and shorter in the triatomics. Using the Herschbach and Laurie-type empirical rule correlating r_e and F_{CoO} developed for CoO,[9] we suggest $r_e(OCoO) = 1.615 \pm 0.010$ Å (Table 4).

It is interesting to compare these results to those obtained previously on the Ni + O_2 system. Both systems form linear dioxides as most stable states for the one-on-one M/O_2 reaction, and we are now certain that the transition from bent to linear structures in the OMO series happens earlier in the row.[18] In the Ni + O_2 system, however, formation of a cyclic Ni−O_2 intermediate step in the reaction was clearly evidenced.[8] It seems

TABLE 4: Vibrational Harmonic Frequencies (cm^{-1}) and Isotopic Shifts (in Parentheses for $^{16}OCo^{18}O$ and $^{18}OCo^{18}O$) Calculated with the CCSD(T) and BPW91 Functional Methods and Various Extended Basis Sets

methods	ν_1	ν_2	ν_3
CCSD(T)/6-311G(3df)	778.0 (−24.1, −44.6)	129.8 (−2.3, −4.8)	991.1 (−16.4, −36.4)
Lin (6311+G(2d))	888.3 (−28.4, −51.0)	87.3i	1036.5 (−16.0, −38.1)
Bent(6311+G(2d))	898.9 (−27, −50.0)	113 (−2.2, −4.4)	1074.1 (−17.4, −40.0)
Lin (6311G(2d))	913.3 (−29.0, −52.3)	55.8 (−1, −2.1)	1080.8 (−17.0, −39.0)
Lin (6311G(3df))	935	59	1098
Lin (6311G(3df), DKH)	950.5 (−30.3, −54.4)	73.4 (−1.3, −2.7)	1114.0 (−17.4, −41)
exptl in RG[a]	796.2 (−25.1, −44.7)[b]	82.8 (−1.5, −4)[c]	954.7 (−13.5, −34.0)[a]

[a] Uncorrected for anharmonicity. [b] In solid neon. [c] In solid argon. ±1 cm^{-1} uncertainty on isotopic shifts.

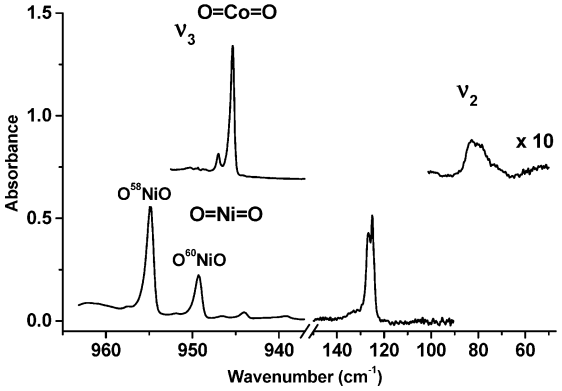

Figure 7. Comparison of the asymmetric stretches (ν_3) and bending modes (ν_2) of OCoO and ONiO in solid argon.

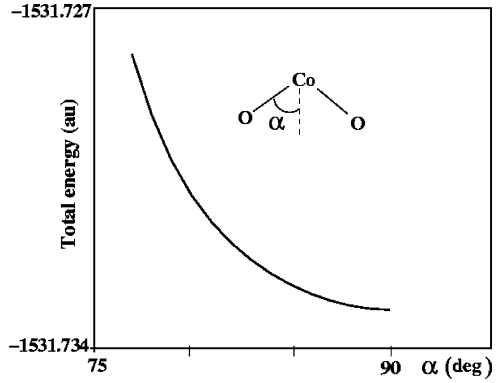

Figure 8. Potential energy profile (PEF) of OCoO ($^2A_1$) as a function of the OCoO half-bond-angle (α) at the CCSD(T)/6-311G(3df) level.

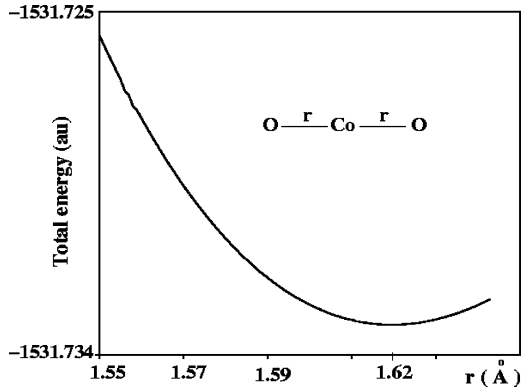

Figure 9. Potential energy profile (PEF) of OCoO ($^2\Sigma_g^+$) as a function of the O−Co bond length at the CCSD(T)/6-311G(3df) level.

that the near-degeneracy between states arising from the $3d^8$-$4s^2$ and $3d^94s^1$ configurations might provide a clue to this difference. For Co, the larger energy difference between $3d^7$-$4s^2$ and $3d^84s^1$ imposes a small energy barrier to the reaction. The symmetric ν_1 and asymmetric ν_3 stretching modes have very close frequencies in ONiO and OCoO, and the Ni−O and Co−O bond force constants are only slightly different, but stronger in both cases than in the respective diatomic molecules (Table 4). The bending modes have, however, quite different energies and, also, different absorption profiles and intensities (Figure 7). The bending mode fundamental in OCoO is both lower and eight times weaker than in ONiO. This observation cannot be attributed to a mass effect, and it seems more likely that the extra electron inducing the change from $^2\Sigma$ to $^1\Sigma$ plays an important role in the rigidity of the molecule and the electric dipole modulation upon bending.

Theoretical Calculations

As discussed previously, a theoretical study of the electronic structure of cobalt dioxide is a difficult task. All of the DFT-based calculations have predicted a bent structure for the doublet state,[4−7] while Bauschlicher et al. at the CASSCF level found the $^2\Delta_g$ state below the $^2\Sigma_g^+$ state by 1487 cm^{-1}.[4] To suggest a theoretical description coherent with the available experimental data, we reinvestigate this topic first at the CCSD(T) and next at the DFT levels of theory. Our strategy is to find methods which are able to reproduce, even qualitatively, the geometry and electronic structure and to apply them to the calculations of potential energy surfaces (PES) and the investigations of a reaction pathway.

A free and total optimization was not achieved even with extensive CPU time because of the complexity of the problem arising from the many low-lying PESs: For a given C_{2v} symmetry, several doublet states of different symmetries can be accessed. The procedure used was thus as follows: The lowest doublet state was first determined within the doublet manifold at a fixed geometry ($^2A_1$), examining the potential energy and electronic density and structure using the data provided in the checkpoint file (*.chk) provided by the Gaussian program. Next, the angular parameter (α) was scanned, with the constraint of staying on the same PES, which is checked for each point. In a third step, while controlling through *.chk values that the molecule remains on the same PES, the bond length is reoptimized. At the CCSD(T) level, it is clear that the surface correlating with the $^2\Delta_g$ state is located at higher energy in the vicinity of linearity. Figures 8 and 9 display the potential energy profiles (PEFs) calculated at the CCSD(T)/6−311(3df) level. As shown in Figure 8, the energy on the $^2A_1$ surface converges slowly toward the linear structure and the $^2\Sigma_g^+$ state. When the PEF is calculated as a function of the Co−O distance, remaining on the $^2\Sigma_g^+$ surface, the minimum is reached near 1.620 Å, close to the experimental suggestion (Figure 9). The vibrational frequencies are reported in Table 4, giving an excellent agreement on the stretching modes but an overestimated value for the bending frequency. As the quality of the results obtained using these methods is basis set-dependent, further calculations using a larger basis set should improve the situation. Next, we tested several approaches using DFT

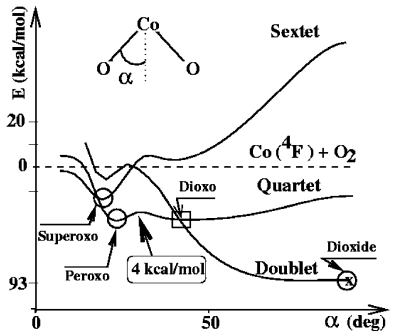

Figure 10. Potential energy profiles of the Co + O_2 interaction evolving in the $^6A_1$, $^4A_1$, and $^2A_1$ surfaces as a function of the OCoO half-bond-angle (α) at the BPW91/6-311G(2d) level.

methodology in order to find a method capable of yielding qualitatively correct results in comparison with experimental and CCSD(T), but still practicable for larger systems than the triatomics. We present a more complete study of the Co + O_2 reaction using the BPW91 functional. This functional yielded slightly better results here, a choice which was also justified in previous works.[5,21] States of doublet, quartet, and sextet multiplicities have also been recalculated at the BPW91/6-311+G(2d) level, and we found the structures for dioxo molecules in the sextet and quartet manifolds at higher energies. In particular, the $^6A_1$ state predicted as the ground state in refs 6 and 7 is calculated here to be 0.7 eV above the doublet ground state. At this level, our results are comparable to those of ref 5, namely a $^2A_1$ minimum with $2\alpha = 155°$, with the linear structure corresponding to the inversion transition state, calculated here to be 138 cm^{-1} above either minimum. As mentioned before, this is neither in line with the ESR results nor compatible with the IR data (the ν_1 mode would be predicted with a sizable intensity, for instance).

First, we wish to note that, in transition metal dioxides, the bonding is largely dominated by the ionic contribution because of the oxidative character of the compound. Test calculations showed that the use of diffuse functions in the atomic basis sets, added to improve the description of covalent compounds, enhance and, perhaps, overestimate the covalent contribution in the polyatomic transition metal oxides. Here, using 6-311G basis set augmented only by polarization functions (2d and 3df), the OCoO geometry converges slowly toward a linear $^2\Sigma_g$ structure. A vibrational frequency calculation then clearly shows that it is a stationary point without any imaginary frequency (Table 4).

Second, we present in Figure 10 the evolution of the Co + O_2 interaction on the A_1 surfaces correlating with the $^2\Sigma_g^+$ ground state. Our starting point corresponds to the system on the sextet surface (^{4}F state for Co and $^3\Sigma_g$ for O_2). We made sure that the electronic configuration of Co corresponds to that of the b^{4}F state ($3d^84s^1$). To avoid size consistency problems, the dissociation energy limit was calculated with the two subunits placed at a very large distance apart (10 Å). From the entrance channel in the reaction, we can obtain a $^6A_1$ metastable triangular structure. As shown in Figure 11, the O−O bond length is close to a typical distance in superoxo complexes.[22] Very near the bottom of the sextet minimum, intersystem crossing with the $^4A_1$ PEF occurs, meaning that the sextet state cannot be stabilized in this picture. Consequently, the Co(^{4}F) + O_2 ($^3\Sigma_g$) system goes without an energy barrier to the first minimum of the quartet surface (noted peroxo on Figure 11, on account of the elongated O−O distance). At this level, the system in the quartet peroxo state could go to the next quartet

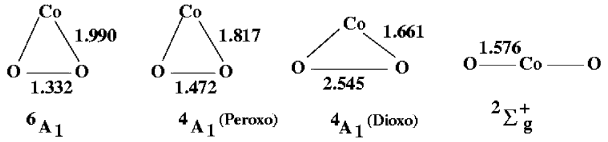

Figure 11. Geometric parameters for different states calculated at the BPW91/6-311G(2d) level. All distances are in Å.

state (dioxo on Figure 11) slightly lower in energy, if the system has enough internal energy to overcome a small energy barrier of 4 kcal/mol. In regard of the 25 kcal/mol heat of reaction in the preceding step, the process is again probable. Close to the quartet dioxo minimum, the $^4A_1$ PEF crosses the $^2A_1$ one, leading then without an energy barrier to the ground state of the overall reaction ($^2\Sigma_g^+$). At this level, the ground-state bond length is calculated to be 1.576 Å, some 0.04 Å shorter than the estimated value. Consequently, both stretching frequencies are overestimated (Table 4), a trend which is increased at the BPW91/6-311G(3df) level where the CoO bond shrinks even further (1.569 Å), also when using scalar relativistic correction (1.561 Å).

Conclusions

In this paper, we report new experimental and theoretical data on the one-on-one reaction pathway and reaction products of atomic cobalt and molecular oxygen isolated in argon and neon matrices. As in the gas phase,[3] the Co + O_2 system is found to be nonreactive in the ground state but strongly reactive in the first excited state about 4000 cm^{-1} above the ground state and, then, more weakly reactive after excitation near 7400 cm^{-1} at energies corresponding to the first two excited states of Co (b^{4}F and a^{2}F). The reactivity of the Co atom in its b^{4}F ($3d^84s^1$) state with O_2, and the inertness of the ground state ($3d^74s^2$ configuration) can be compared to that observed in the Co + CO reaction in solid argon[23] or in the reaction of a gas-phase transition metal atom with $3d^n4s^2$ configurations.[24] Absorptions previously assigned to superoxo or peroxo forms of Co(O_2) belong to larger species, and the only Co + O_2 reaction product observed is the insertion dioxo form, OCoO. Finally, the linear structure of OCoO can be confirmed, at least in rare gas matrices, after observation of the ν_2 bending mode at 82.8 cm^{-1} and the ν_1 symmetric stretch for the $^{16}OCo^{18}O$ isotopomer at 760.4 cm^{-1}. In addition to the observation of the $\nu_1 + \nu_3$ combination yielding the $X_{13} = -11.7$ cm^{-1} crossed anharmonicity term, the ν_1 stretch of $^{16}OCo^{16}O$ can be placed at 783.7 ± 0.5 cm^{-1} in argon and 796.2 ± 0.5 cm^{-1} in neon, in excellent agreement with observations in photodetachment spectroscopy studies[17] (790 ± 60 cm^{-1}). Comparison of the CoO force constant with the empirical correlation made for CoO estimates r_e = 1.615 ± 0.01 Å bond length in OCoO. CCSD(T) calculations are presented and are in line with experimental observations. New DFT calculations have also been carried out with extended basis sets in the absence of diffuse atomic functions, which can be favorably compared to the CCSD(T) and experimental results. These DFT-based calculations are then used to provide a realistic proposal for the reaction pathway.

Acknowledgment. We thank Danielle Carrère for her careful assistance in preparing the experiments. This work was supported by C.N.R.S. Grant UMR 7075 and Plan Pluri-Formation of the University Pierre et Marie Curie. M.E.A. acknowledges allocation of supercomputer time at IDRIS (CNRS, grant 041730).

References and Notes

(1) Valeri, S.; Borghi, A.; Gazzadi, G. C.; di Bona, A. *Surf. Sci.* **1999**, *423*, 346.

(2) Van Zee, R. J.; Hamrick, Y. M.; Li, S.; Weltner, W., Jr. *J. Phys. Chem.* **1992**, *96*, 7247.

(3) Matsui, R.; Senba, K.; Honma, K. *J. Phys. Chem. A* **1997**, *101*, 179.

(4) Chertihin, G. V.; Citra, A.; Andrews, L.; Bauschlicher, C. W., Jr. *J. Phys. Chem. A* **1997**, *101*, 8793.

(5) Gutsev, G. L.; Rao, B. K.; Jena, P. *J. Phys. Chem. A* **2000**, *104*, 11961.

(6) Uzunova, E. L.; Nikolov, G. St.; Mikosh, H. *J. Phys. Chem. A* **2002**, *106*, 4104.

(7) Uzunova, E. L.; Nikolov, G. St.; Mikosh, H. *ChemPhysChem* **2004**, *5*, 192.

(8) Danset, D.; Manceron, L.; Andrews L. *J. Phys. Chem. A* **2001**, *105*, 7205.

(9) Danset, D.; Manceron, L. *J. Phys. Chem. A* **2003**, *107*, 11324.

(10) Frisch, M. J.; Trucks, G. W.; Schlegel, H. B.; Scuseria, G. E.; Robb, M. A.; Cheeseman, J. R.; Montgomery, J. A., Jr.; Vreven, T.; Kudin, K. N.; Burant, J. C.; Millam, J. M.; Iyengar, S. S.; Tomasi, J.; Barone, V.; Mennucci, B.; Cossi, M.; Scalmani, G.; Rega, N.; Petersson, G. A.; Nakatsuji, H.; Hada, M.; Ehara, M.; Toyota, K.; Fukuda, R.; Hasegawa, J.; Ishida, M.; Nakajima, T.; Honda, Y.; Kitao, O.; Nakai, H.; Klene, M.; Li, X.; Knox, J. E.; Hratchian, H. P.; Cross, J. B.; Adamo, C.; Jaramillo, J.; Gomperts, R.; Stratmann, R. E.; Yazyev, O.; Austin, A. J.; Cammi, R.; Pomelli, C.; Ochterski, J. W.; Ayala, P. Y.; Morokuma, K.; Voth, G. A.; Salvador, P.; Dannenberg, J. J.; Zakrzewski, V. G.; Dapprich, S.; Daniels, A. D.; Strain, M. C.; Farkas, O.; Malick, D. K.; Rabuck, A. D.; Raghavachari, K.; Foresman, J. B.; Ortiz, J. V.; Cui, Q.; Baboul, A. G.; Clifford, S.; Cioslowski, J.; Stefanov, B. B.; Liu, G.; Liashenko, A.; Piskorz, P.; Komaromi, I.; Martin, R. L.; Fox, D. J.; Keith, T.; Al-Laham, M. A.; Peng, C. Y.; Nanayakkara, A.; Challacombe, M.; Gill, P. M. W.; Johnson, B.; Chen, W.; Wong, M. W.; Gonzalez, C.; Pople, J. A. *Gaussian 03*, revision B.01; Gaussian, Inc.: Pittsburgh, PA, 2003.

(11) Becke, A. D. *Phys. Rev. A* **1988**, *38*, 3098.

(12) Perdew, J. P.; Wang, Y. *Phys. Rev. B* **1992**, *45*, 13244.

(13) Krishnan, R.; Binkley, J. S.; Seeger, R.; Pople, J. A. *J. Chem. Phys.* **1980**, *72*, 650.

(14) Clark, T.; Chandrasekhar, J.; Spitznagel, G. W.; Schleyer, P. V. R. *J. Comput. Chem.* **1983**, *4*, 294.

(15) Frisch, M. J.; Pople, J. A.; Binkley, J. S. *J. Chem. Phys.* **1984**, *80*, 3265.

(16) Mann, D. M.; Broida, H. P. *J. Chem. Phys*, **1971**, *55*, 84.

(17) Wang, L. S. Unpublished results cited in ref 4.

(18) Andrews, L.; Chertihin, G. V.; Ricca, A.; Bauschlicher, C. W., Jr. *J. Am. Chem. Soc.* **1996**, *118*, 467.

(19) Namiki, K. C.; Saito, S. *J. Chem. Phys.* **2001**, *114*, 9390.

(20) Ram, R. S.; Jarman, C. N.; Bernath, P. F. *J. Mol. Spectrosc.* **1993**, *160*, 574.

(21) Gutsev, G. L.; Rao, B. K.; Jena, P. *J. Phys. Chem. A* **2000**, *104*, 5374.

(22) Hall, M. B. In *Oxygen Complexes and Oxygen Activation by Transition Metals*; Martell, A. E., Sawyer, D. T., Eds.; Plenum: New York, 1988; pp 3−16.

(23) Tremblay, B.; Alikhani, M. E.; Manceron, L. *J. Phys. Chem. A* **2001**, *105*, 11388.

(24) Mitchell, S. In *Gas-Phase Metal Reactions*; Fontijn, A., Ed.; Elsevier: Amsterdam, 1992; p 227−252.